Understanding The Dynamics Of Vapor Intrusion Processes

Brown University

Jonathan G. V. Ström

Spring 2020

Contents

Chapter 1

Numerical Modeling of Vapor Intrusion

Abstract

Vapor intrusion (VI) investigations, the effort to determine the exposure and associated human health-risk at a VI impacted building, are often complicated by significant spatial and temporal variability in VI. Over the years there have been efforts to develop new techniques and methodologies that aim to reduce the issues associated with these variabilities; simplifying and improving the robustness of VI site investigations. The development of the controlled pressure method (CPM), where the pressurization of a building is controlled to increase or decrease contaminant entry into the building, is one such example. Another approach is to use indicators, tracers, and surrogates (ITS) to help guide when to conduct site investigations, ideally increasing the likelihood of determining the higher indoor contaminant concentrations.

Both of these approaches rely on a quasi-deterministic relationship between some external variable, such as building pressurization, and indoor contaminant concentration. However, site-specific conditions can give rise to very different responses to such an external variable, and to effectively use CPM or ITS, a better mechanistic understanding of contaminant transport and exposure are needed.

In this thesis, we develop three-dimensional finite element models of VI impacted buildings from a first principles perspective. These models combined with analysis of field data from VI sites, allows us to explore the physical mechanisms that drive VI. By considering the dominant contaminant transport mechanism at a site, e.g. if advective or diffusive transport dominates, we can explain why a change in building pressurization can lead to such differences in contaminant concentration at different sites. We can also better understand how various factors in VI contribute to the overall variability.

By classifying the dominant contaminant transport mechanism at a site, we can more effectively anticipate how a particular site will respond to some external stimuli. This will in turn reduce the effort required to, and increase the robustness of the techniques used determine the relevant human exposure at a VI site.

1.1 Introduction

To formulate a mathematical description of VI, we consider a simple hypothetical VI scenario at steady-state and develop a three-dimensional model of this. Consider a VI impacted house with a 10 m by 10 m footprint with a basement whose foundation lies 1 m below ground surface (bgs). There is also a 1 cm wide crack along the perimeter of the 15 cm thick foundation, where all contaminant entry into the house is assumed to occur. Here we will consider the basement as the control volume for which the indoor contaminant concentration will be determined. It is assumed to have a ceiling height of 3 m, giving a total volume of $300\,\mathrm{m}^3$ and that contaminant vapors are expelled via air exchange with the exterior; the air exchange rate is assumed to be $0.5\,\mathrm{h}^{-1}$.

The contaminant source is to be the underlying groundwater, which is assumed to be 4 m bgs, and infinitely and homogenously contaminated with $0.1\,\mathrm{mol\,m}^{-3}$ of TCE, i.e. the groundwater contaminant concentration does not change over time nor does it have any concentration gradients. We will only consider contaminant transport in the portion of soil between the open ground surface and the groundwater interface - the *vadose zone*. This soil is assumed to be homogenous and consist only of *sandy loam* type soil, i.e. there no soil layers, rocks, etc. For now, we will assume that no contaminant sorption into/onto the soil occurs, but this phenomena will be explored in Chapter (TBD).The house is assumed to be surrounded by open ground that extend 10 m from the house wall. Contaminant concentration in the atmosphere is assumed so low that is effectively zero, and thus contaminant vapors that reach the ground surface are immediately infinitely diluted, i.e. goes to zero.

The house interior is assumed to be slightly depressurized relative to ambient due to the stack effect; the indoor/outdoor pressure difference is $-5\,\mathrm{Pa}$ This induces an airflow from the ground surface, through the soil, and into the house via the foundation crack. The airflow combined with contaminant diffusion and evaporation from the groundwater gives the contaminant transport in the soil. Figure 1.1 shows a figure summarizing this VI scenario.

The indoor environment will be modeled as a continuously stirred tank reactor (CSTR), (but without reactions), where the indoor contaminant concentration will depend on the contaminant entry rate n_{ck} from the soil via the foundation crack and the air exchange rate A_e. The details of this will be covered section 1.3.1.

To determine n_{ck} the contaminant transport in the soil needs to be modeled. This will be done by the advection-diffusion equation, which will be modified for transport in soils. The contaminant transport itself is driven by a concentration gradient and airflow in the soil. The contaminant source (groundwater) and sink (atmosphere and contaminant entry into the building) will largely determine the concentration gradient here, while the airflow needs to be calculated separately. Details are covered in section 1.3.4.

The airflow in the soil is modeled by Darcy's Law, and is driven by a pressure gradient in the soil, which induced by the indoor/outdoor pressure difference. Details are in section 1.3.3.

One last consideration is that the vadose zone is partially saturated with water, with the soil pores more or less filled near the groundwater interface, with soil moisture content decreasing as a function of elevation above groundwater z [m]. The soil moisture content has a profound effect on transport in the soil; it restricts

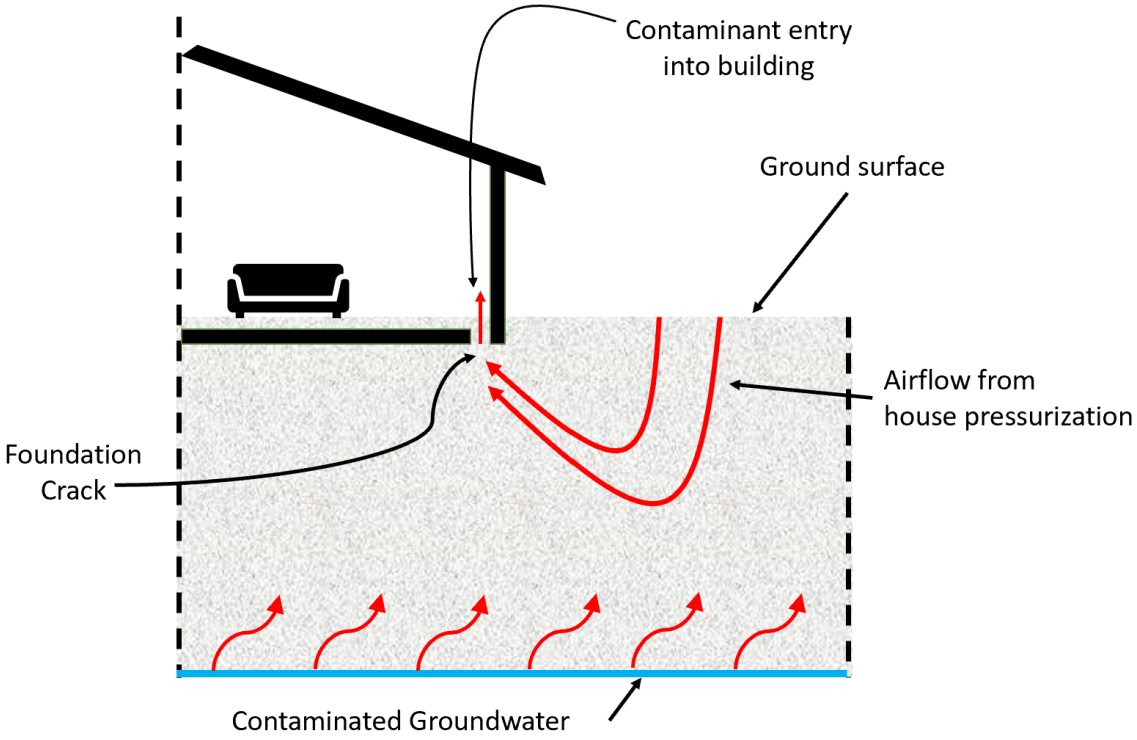

Figure 1.1: The considered VI scenario.

the airflow and contaminant diffusivity in the soil. Thus, the soil moisture content θ_w must be determined first in order to solve the contaminant transport and Darcy's Law.

The resulting physical system is highly coupled, with many of the physics depend on the solution of each other. Figure 1.2 shows the coupling between each physics, its output, and how it relates to the other physics to ultimately determine VI.

In this chapter, we will go walkthrough the process of numerically modeling this VI scenario using the finite element method (FEM) and post-processing of the results. A discussion regarding past and present VI models, their advantages and limitations, will follow.

1.1.1 Finite Element Method

Most physical phenomena are described by partial differential equations (PDEs), but for anything but the simplest scenarios, these do not have an analytical closed-form solutions; therefore numerical methods are necessary to find an approximate solution. This is achieved by discretizing the problem, i.e. transforming a continuous problem into a discrete one. There are numerous ways to discretize a problem, and some of the more popular schemes are finite difference (FDM), finite volume (FVM), and finite element method (FEM).

In this work we use FEM, which is a popular numerical scheme that offers some distinct advantages over other schemes for modeling VI. FEM subdivides domain of the PDE problem into many smaller subdomains called elements. These elements can take a wide variety of shapes, e.g. tetrahedra, prisms, or cuboids for three-dimensional problems and triangles or rectangles for two-dimensional problems. The

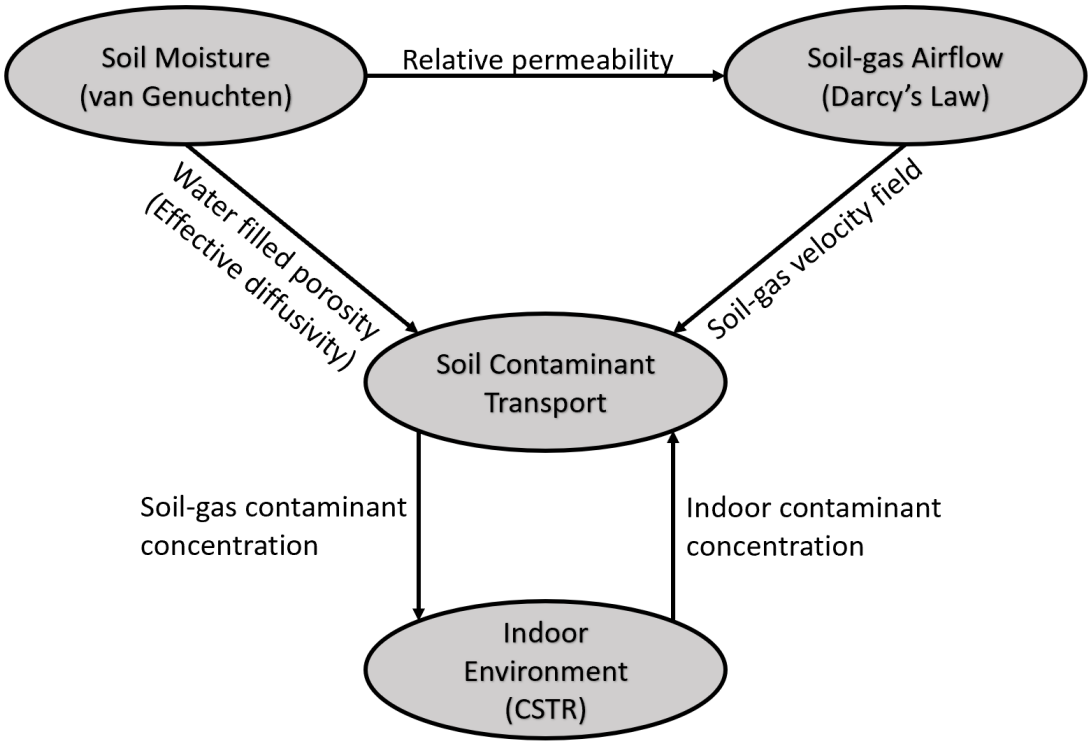

Figure 1.2: Coupling between the physics used to model VI.

collection of elements that make up the domain or geometry is called a *mesh*. The fineness of the mesh is what largely determines the accuracy of the solution, but also increases the computational costs.

The size of each element can be highly ununiform which allows FEM to discretize complicated geometries. This is advantageous for modeling VI, where different parts of the geometry can have dramatically different resolution requirements; the 1 cm foundation crack requires elements on the scale of mm, while in other parts of the geometry the resolution requirement is on the scale of m. This ability to easily represent complicated geometries with elements of ununiform sizes helps maintain accuracy while saving computational resources. Another benefit of using these elements is that it is easy to assign different constant values throuhout the domain, and heterogenous materials can easily be represented.

The purpose of this work is not to provide a detailed description of the FEM, but for the interested reader Larson and Bengzon[1] is a good resource. However, it is important to know that FEM assumes that the approximated solution to a PDE can be written as a series of linear functions, called *basis functions*.

$$u \approx u_h = \sum^{i} u_i \psi_i \tag{1.1}$$

here u is the exact solution to the problem; u_h is the approximate solution; u_i is a *nodal coefficient*; and ψ is a *basis function*. These basis functions are usually some simple function, e.g. a hat function or some lower-order polynomial.

These basis functions are used to discretize the problem by rewriting a PDE into its *weak form*, multiplying the equation with another set of functions called a *test function*. The test functions are the same type of function as the basis function, i.e.

if the basis function is a hat function, so is the test function. The result of this is an integral, where the integrands are the product of the basis function. These integrals are numerically solved using some quadrature method, which gives a linear system of equations. This system of equations is then solved to give all of the u_i coefficients and thus the approximated solution u_h.

The point of this is that choice of basis function, i.e. hat function, first or third order polynomial, can influence the accuracy of the solution, and certain basis functions are more appropriate for certain PDEs. Generally, higher order polynomials will give a more accurate solution, but at a computational cost, making it sometimes difficult to choose. This adds another level of complexity of using FEM over some other numerical schemes, as the accuracy of the solution is not only influenced by the mesh but also somewhat by the choice of basis functions. This highlights one of the drawbacks of FEM, i.e. that it is mathematically more challenging to implement and use than some other numerical schemes may be.

Fortunately, due to the attractiveness of the method, many commercial FEM packages have developed which increases usability significantly. In this work we will use such a package - COMSOL Multiphysics, where subsequent sections will cover the steps required to implement our VI model in COMSOL. (Of course, this could easily be translated into use in another software package.)

In order, we will cover:

1. Creation of a model geometry.
2. Defining physics/governing equations, boundary, and initial conditions.
3. Discretize/mesh the geometry.
4. Solver configuration.
5. Post-process the results.

1.2 Geometry Generation

Designing a good model geometry is critical as it can save significant computational resources. When designing a geometry the FEM user should try to represent the model geometry as accurately as possible while:

1. Avoid unnecessarily fine details; these may require an excessively fine mesh to resolve.
2. Leverage symmetry to reduce geometry size and thereby the mesh.

Achieving these goals is not always straightforward, and depend on the skill of the modeler and on the available tools. Typically a model geometry is constructed in some computer assisted design (CAD) software, and the particular tools available in these vary by software.

COMSOL has a built-in geometry generation tool, which allows the construction of advanced geometries by performing various operations on simpler geometries, e.g. a cylinder and half sphere can be combined to make a rivet. It is also possible to import pre-generated geometries from other CAD software. However, we will create our own geometry.

The interior, or indeed the house itself will not be explicitly modeled, instead we will only consider the soil surrounding the house. This is done for the simple reason that interiors are simply too heterogenous to generalize in any meaningful way. Even if the interior was explicitly modeled, it would be prohibitively expensive to do, as it would require solving the Navier-Stokes equation. Instead the interior is implicitly modeled as a CSTR and simply coupled with the explicit geometry via the foundation crack boundary.

One of the nice properties of our VI scenario is that, due to symmetry, we only need to explicitly model a quarter of it. This reduces the number of required mesh points by 75%, which is a huge computational saving. To create our quarter geometry, only a few simple geometric objects and Boolean operations are required: two cuboids, two rectangles, one Boolean difference operation, and one Boolean join operation. Figure 1.3 shows the resulting geometry. Note that $z = 0\,\mathrm{m}$ is the groundwater/soil interface and the plane of symmetry is around the $(x, y) = (0\,\mathrm{m}, 0\,\mathrm{m})$ axis

To create the soil surrounding the building:

1. Create a 15 m by 15 m by 4 m block with its base at $(x, y, z) = (0\,\mathrm{m}, 0\,\mathrm{m}, 0\,\mathrm{m})$. This is the entire soil domain.

2. Create a 5 m by 5 m by 1 m block with its base at $(x, y, z) = (0\,\mathrm{m}, 0\,\mathrm{m}, 3\,\mathrm{m})$. This will represent the volume that the house take up in the soil, i.e. the underground portion of the basement.

3. Perform a difference operation, removing the "basement" block from the "soil" block.

At this point you will see that a quarter soil domain has been created, with an empty space that represents a house with a foundation slab located 1 m bgs.

The foundation crack will be modeled by joining two 1 cm wide strip that spans the perimeter of the surface that represents the house foundation. This strip is created by joining two rectangles on foundation surface:

1. Define a work plane 3 m above zero. This allows us to place two-dimensional objects on the surface of or inside a three-dimensional object.

2. On the work plane create a 5 m by 1 cm rectangle with its base at $(x, y) = (0\,\mathrm{m}, 5\,\mathrm{m} - 1\,\mathrm{cm})$. This represents one side of the perimeter crack.

3. Copy the rectangle and rotate it 90° around the corner of the foundation, i.e. $(x, y) = (5\,\mathrm{m} - 0.5\,\mathrm{cm}, 5\,\mathrm{m} - 0.5\,\mathrm{cm})$.

4. Join the two rectangles to create a unified perimeter foundation crack.

Now the geometry of this VI scenario is complete.

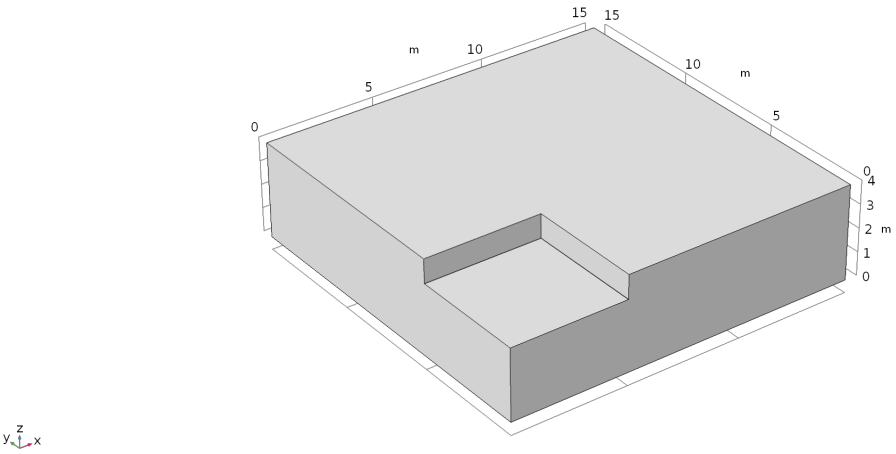

Figure 1.3: The complete geometry of the VI scenario.

1.3 Vapor Intrusion Physics & Govering Equations

1.3.1 The Indoor Environment

The indoor air space is perhaps the most important part of modeling VI, as the goal of these models ultimately is to predict indoor exposure given some external factors. The indoor environment is modeled implicitly as a continuously stirred tank reactor (CSTR).

We assume that all contaminant entry (or exit) into the house occurs via the foundation crack. Once the contaminant enters the interior, it is instantly perfectly mixed, which is a key assumption of a CSTR. Contaminant expulsion occurs via air exchange with the outdoor environment, and is regulated by *air exchange rate* A_e, which dictates which portion of the indoor air is exchanged with the outdoor for a given period of time. For instance, a common air exchange rate for a house is $0.5\,\mathrm{h}^{-1}$, i.e. half of the indoor air is exchanged every hour. It should be noted that in this simple VI model implementation, we assume that there are no indoor sources nor that any sorption to/from any indoor materials occurs. Thus, the reaction term that would ordinarily be part of a CSTR is dropped (but is reintroduced in Chapter (TBD)) and the change in indoor contaminant concentration is thus given by (1.2).

$$V_{\mathrm{bldg}}\frac{\partial c_{\mathrm{in}}}{\partial t} = n_{\mathrm{ck}} - V_{\mathrm{bldg}}A_e c_{\mathrm{in}} \tag{1.2}$$

Here c_{in} $[\mathrm{mol\,m^{-3}}]$ is the indoor air contaminant concentration; n_{ck} $[\mathrm{mol\,s^{-1}}]$ is the contaminant entry (or exit) rate into the building via the foundation crack; $A_e = 0.5\,\mathrm{h}^{-1}$ is the air exchange rate; Finally, $V_{\mathrm{bldg}} = 300\,\mathrm{m}^3$ is the volume of the house interior (or basement in this case).

A limitation of this approach is that we only consider one control volume or compartment, while in reality indoor contaminant concentrations can vary significantly between compartments, in particular between different floors. There are VI models that use multiple compartments, which in essence are just coupled CSTRs[**murphy˙multi-compartment˙2011**]. Basements typically have higher indoor contaminant concentrations than other floors, so in this implementation we

assume that our sole compartment is the house basement, which $V_{\text{bldg}} = 300\,\text{m}^3$ reflects.

Solving (1.2) requires us to determine the contaminant entry and air exchange rate. Air exchange rates can vary quite significantly, and are a significant source of temporal variability in VI, a topic that will be further explored in Chapter (TBD). However, they typically vary around relatively well-known values as air exchange rates are regulated in building codes. For residential homes, it is typical that air exchange rate is around $A_e = 0.5\,\text{h}^{-1}$ and thus for simplicity we will choose this value.

Contaminant entry into the building Contaminant entry rates are significantly more difficult to determine, as they depend on air velocity through the foundation breach and the concentration gradient across it. The determination of these is the main point, and challenge of VI modeling.

The contaminant entry n_{ck} is given by integrating the contaminant entry flux j_{ck} across the foundation crack boundary A_{ck}.

$$n_{\text{ck}} = \int_{A_{\text{ck}}} j_{\text{ck}} dA \tag{1.3}$$

The contaminant flux across the foundation crack is modeled as transport between two parallel plates and has an advective and a diffusive component.

$$j_{\text{ck}} = j_{\text{advection}} + j_{\text{diffusion}} \tag{1.4}$$

Since indoor contaminant concentration is lower than they are in the soil or near foundation crack region a concentration gradient from the soil-gas to the indoor will be present. The interior of the crack is not explicitly modeled, but assumed to only contain air and thus we assume the diffusion coefficient is the same as in air.

$$j_{\text{diffusion}} = -\frac{D_{\text{air}}}{L_{\text{slab}}}(c_{in} - c_g) \tag{1.5}$$

here $D_{\text{air}} = 7.2 \times 10^{-6}\,\text{m}^2\,\text{s}^{-1}$ is the diffusion coefficient of TCE in air (but could be substituted for any contaminant of interest); $L_{\text{slab}} = 15\,\text{cm}$ is the thickness of the foundation slab; c_{in} $[\text{mol}\,\text{m}^{-3}]$ is the indoor contaminant concentration; c_g $[\text{mol}\,\text{m}^{-3}]$ is the contaminant gas-phase concentration at the foundation crack boundary.

Advective transport through the slab can occur in both directions, i.e. contaminants can be carried from the soil into the house and from the house into the soil[2]. The direction of this transport depend on the direction of the flow, with a positive sign indicating that airflow goes into the house.

$$j_{advection} = \begin{cases} u_{ck} c_g & u_{ck} \geq 0 \\ u_{ck} c_{in} & u_{ck} < 0 \end{cases} \tag{1.6}$$

here u_{ck} $[\text{m}\,\text{s}^{-1}]$ is the airflow velocity through the foundation crack.

Thus the total contaminant transport through the foundation crack is given by (1.7).

$$j_{ck} = \begin{cases} u_{ck} c_g - \frac{D_{\text{air}}}{L_{\text{slab}}}(c_{in} - c_g) & u_{ck} \geq 0 \\ u_{ck} c_{in} - \frac{D_{\text{air}}}{L_{\text{slab}}}(c_{in} - c_g) & u_{ck} < 0 \end{cases} \tag{1.7}$$

Not only will (1.7) be used to calculate the contaminant entry rate into house, but is a necessary boundary condition for calculating the contaminant concentration in the soil. However, as we see, (1.7) is a function of both the soil-gas concentration at the foundation crack boundary c_g and the indoor contaminant concentration cin, thus these two are coupled and needs to be solved simultaneously.

1.3.2 Variable Soil Moisture Content

The portion of soil between groundwater and ground surface is variably saturated with water and is called the vadose zone. Under environmental conditions, TCE and many other contaminants are miscible in water, and will be partitioned between its dissolved and vapor phases, which has profound effects on the total contaminant transport in the vadose zone. The rates of diffusion in liquids and gases usually differ by orders of magnitudes. Likewise, advective transport in the two phases are vastly different, and as such it is important to account for the varying soil moisture content.

Water filling of soil pores from groundwater is driven by a negative pressure gradient induced by surface tension, called capillary potential and is here represented by ψ. This capillary potential is a function of the soil moisture content, and becomes increasingly negative as the water content decreases, and is zero when the soil matrix is saturated with water. The capillary potential varies with the hydraulic properties of specific soil types.

In addition to the capillary potential, soil moisture content is driven by a gravitational potential, e.g. groundwater flow in soil. The total soil moisture potential ϕ, is the sum of the capillary and gravitational potentials, here expressed as a pressure head.

$$\phi = \frac{\psi(\theta_w)}{\rho g} + h_{\mathrm{g}} = h + h_{\mathrm{g}} \tag{1.8}$$

where ϕ [m] is the total soil moisture potential (as a pressure head); ψ [Pa] is the capillary potential; h [m] is the capillary potential as a pressure head above the groundwater/soil interface; θ_w is the volumetric moisture content by volume soil, i.e. dimensionless; ρ [$\mathrm{kg\,m^{-3}}$] is the density of water; g [$\mathrm{m\,s^{-2}}$] is the acceleration due to gravity; and h_{g} [m] is the gravitational potential above a reference plane.

In the VI scenario considered here, we assume that there is no gravitational potential, and thus that the soil moisture content is at steady-state. This simplifies the determination of the soil moisture content, which now is entirely determined by the capillary potential ψ, or h in our case.

There are two common methods for modeling the capillary potential, one developed by Brooks and Corey[3] in 1966, and another by van Genuchten[4] in 1980. Both of these are semi-empirical approaches and relies on experimentally determined parameters for a specific soil type to be used. In this work, we only use van Genuchten's method, simply because parameters for a wide variety of soils have been made available by the EPA and may be seen in Table 2.

If the assumption that there is no gravitational potential cannot be made, then the full soil moisture potential ϕ needs to be determined. This is achieved by solving Richard's equation.

van Genuchten's Soil-Water Retention Model

The relationship between capillary pressure and moisture content is called *soil moisture retention*, and is what van Genuchten's method models. Specifically, his method models the water saturation of the soil and is given by (1.9).

$$\mathrm{Se} = \begin{cases} \frac{1}{(1+(\alpha|h|)^n)^m} & h < 0 \\ 1 & h \geq 0 \end{cases} \tag{1.9}$$

here Se is the saturation, which ranges from 0 to 1, where 1 is fully saturated with water; α, m, and $n = \frac{1}{1-m}$ are the empirically determined van Genuchten parameters and can be seen in Table 2; and h [m] is the capillary pressure head, which in this case is the elevation above the groundwater/soil interface.

It is important to note that $\mathrm{Se} = 0$ does not mean that there is no moisture in the soil, but soils retain a small amount of water in the matrix - residual moisture content (which again is soil specific). Thus, the soil moisture content is given by (1.10)

$$\theta_w = \begin{cases} \theta_r + \mathrm{Se}(\theta_t - \theta_r) & h < 0 \\ \theta_t & h \geq 0 \end{cases} \tag{1.10}$$

where θ_w is the volumetric soil moisture content; θ_t is the soil porosity; and θ_r is the residual moisture content.

By extension, the soil gas or air content is given by

$$\theta_g = \theta_t - \theta_w \tag{1.11}$$

An example of the soil saturation and moisture content as a function of pressure head is shown in Figure 1.4. Note the steep decline in moisture content near the groundwater interface - that is the capillary zone and we will see that it presents a significant barrier to contaminant transport from the groundwater in section 1.3.4.

The presence of water in the soil matrix has profound implications for transport as the pore space may be restricted to only one phase. For instance, in the capillary zone, the only possible bulk transport in the water phase, while gas phase transport is impossible. The opposite is true near the ground surface, where most of the pore space consists of air.

Soil already limits transport for a single phase due to its permeability, i.e. it is harder to pump water through a soil columns than a pipe of the same size. This extra phase-specific transport inhibition is modeled as a *relative permability* and is given by (1.12).

$$k_r = \begin{cases} \mathrm{Se}^l\left[1 - \left(1 - \mathrm{Se}^{\frac{1}{m}}\right)\right]^2 & h < 0 \\ 0 & h \geq 0 \end{cases} \tag{1.12}$$

here k_r is the relative permeability for water; and $l = 0.5$ is another van Genuchten parameter.

The relative permeability varies from 0 to 1, where 0 indicates that the soil matrix is completely impermeable to the fluid, while a value of 1 means that there is no additional permeability cost. Since k_r here is relative to water, the gas phase relative permeability is given by $1 - k_r$. Figure 1.5 shows how the relative gas and water permeability varies in the vadose zone.

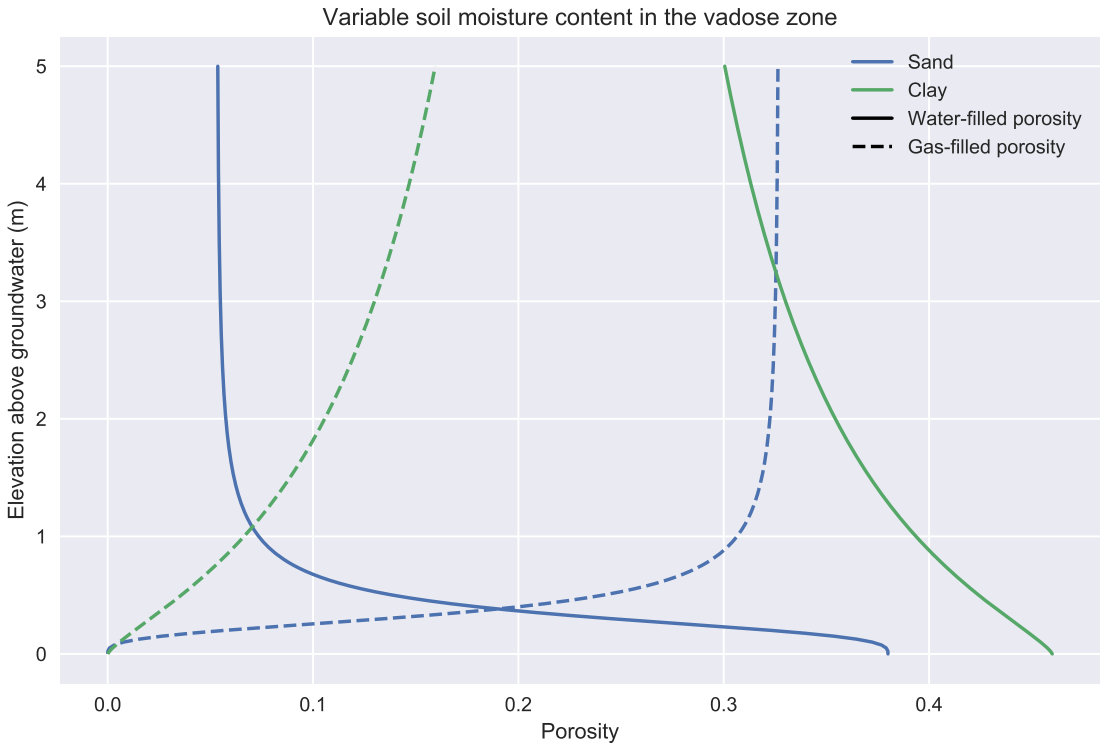

Figure 1.4: Example of a soil moisture retention curve as a function of pressure head above the groundwater/soil interface.

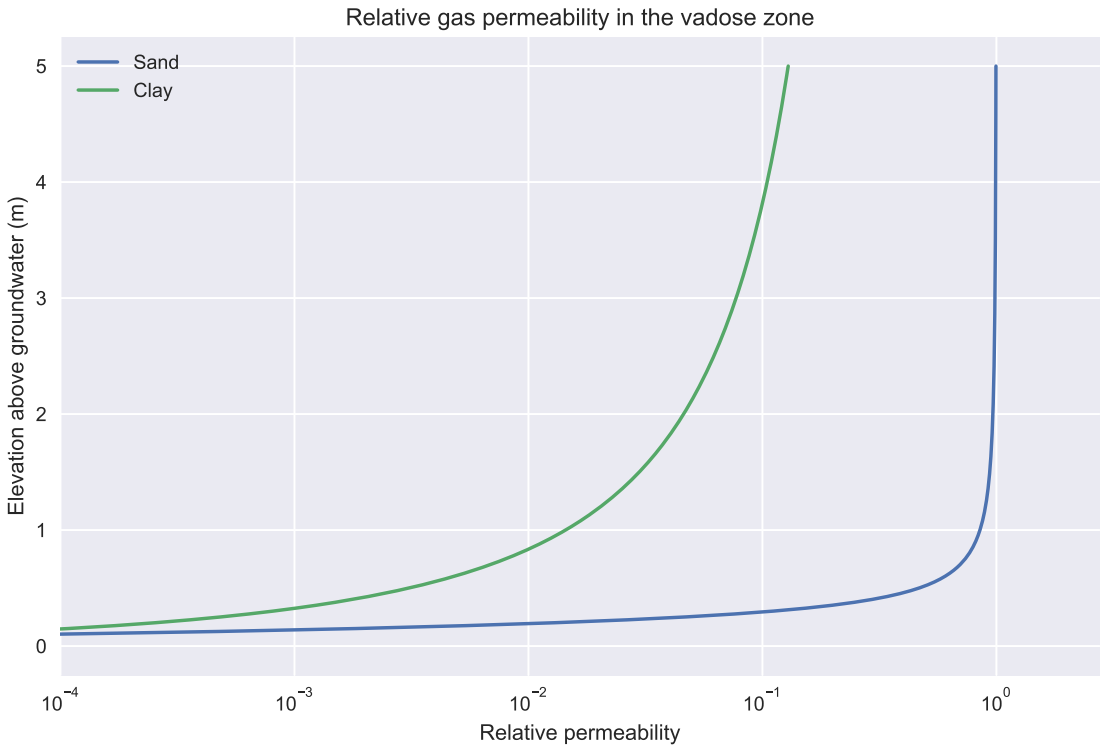

Figure 1.5: Relative gas and water permeability in the vadose zone or above the groundwater interface.

1.3.3 Airflow In The Vadose Zone

In our VI scenario, the depressurized house induces an advective airflow from the ground surface, through the vadose zone, and into the house via the foundation crack, carrying contaminant vapors with it. This airflow is modeled using a modified version of Darcy's Law. The modification is made to account for the variable moisture content in the vadose zone, which is established in section 1.3.2.

Darcy's Law describes the flow of a fluid through a porous medium. This flow is driven by a pressure gradient, and its magnitude depends on the permeability of the porous medium and the fluids viscosity.

$$\vec{u} = -\frac{\kappa}{\mu}\nabla p \tag{1.13}$$

here $\vec{u}$ [$\mathrm{m\,s^{-1}}$] is the airflow velocity vector; κ [$\mathrm{m^2}$] is the permeability of the porous media; μ [$\mathrm{Pa\,s}$] is the dynamic viscosity of the fluid; and ∇ [$\mathrm{Pa\,m^{-1}}$] is the pressure gradient.

This (1.13) formulation of Darcy's Law assumes that the porous media is saturated with the fluid,[1] hence the need to modify this expression. While porosity is not directly part of (1.13), it is an intrinsic property of the permeability κ of the porous media; the variably saturated pores variably changes the permeability. This variation in permeability is modeled using the relative permeability expression from van Genuchten's equation (1.12). The effective soil permeability is the product of the soil permeability and its relative permeability giving our modified Darcy's Law (1.14).

$$\vec{u} = -\frac{(1-k_r)\kappa}{\mu}\nabla p \tag{1.14}$$

Recall that by definition k_r is the relative permeability of the soil to *water* and thus $1 - k_r$ is that to *gas*.

To calculate the soil-gas velocity field in the vadose zone, we need a continuity equation, which for fluid flow is (1.15).

$$\frac{\partial \rho}{\partial t} + \nabla \cdot (\rho \vec{u}) = 0 \tag{1.15}$$

Inserting our modified Darcy's Law for the velocity gives (1.16).

$$\frac{\partial}{\partial t}(\rho\theta_g) + \nabla \cdot \rho\Big(- \frac{(1-k_r)\kappa}{\mu}\nabla p\Big) = 0 \tag{1.16}$$

where θ_g is the gas-filled porosity of the soil from (1.11); $\rho = 1.225\,\mathrm{kg\,m^{-3}}$ is the density of air; and $\mu = 18.5 \times 10^{-6}\,\mathrm{Pa\,s}$ is the dynamic viscosity of air. Contaminant vapor concentrations are typically highly dilute in VI scenarios, and therefore we assume that the contaminant does not affect the transport properties of air.

In order to solve (1.16) we need to define some boundary conditions. In our CSM, air is pulled from the atmosphere through the ground surface and into the building via the foundation crack. To model this only three boundary conditions are required.

[1] Darcy's Law also assumes that the flow is in the laminar regime, i.e. the Reynolds number $\mathrm{Re} < 1$. Due to the small pressure gradients in most VI scenarios, this assumption is rarely unfulfilled, but if it is, then Brinkman's equation should be used instead.

Boundary Conditions The first is to define a pressure gauge, i.e. a reference point for where the pressure is zero, which is where air will be pulled from. This is the applied to the ground surface boundary. The second is that we apply the indoor/outdoor pressure difference (-5 Pa) to the foundation crack boundary. The third type is applied to all remaining boundaries and is a no flow boundary condition, indicating that no flow passes through these boundaries. We also make sure that we specify the symmetry planes present.

$$\text{Ground surface} \qquad p = 0 \text{ (Pa)} \tag{1.17}$$

$$\text{Foundation crack} \qquad p = p_{\text{in/out}} = -5 \text{ (Pa)} \tag{1.18}$$

$$\text{Remaining} \qquad -\vec{n} \cdot \rho\vec{u} = 0 \tag{1.19}$$

where $\vec{n}$ is the boundary normal vector.

Initial Conditions For steady-state problems, the initial conditions do not influence the solution. Transient simulations however, require initial conditions and these are assumed to be given by the steady-state solution.

Basis function A hat function is used as the basis function for solving Darcy's Law in FEM.

1.3.4 Mass Transport In The Vadose Zone

To begin deriving a governing equation for contaminant transport in our VI scenario, we consider the continuity equation which states that the change of concentration in some volume of space depends on the advective and diffusive fluxes in and out of the system, as well as any generation or consumption inside the system.

$$\frac{\partial c}{\partial t} + \nabla \cdot (j_{\text{adv}} + j_{\text{diff}}) - G = 0 \tag{1.20}$$

here c [$\text{mol}\,\text{m}^{-3}$] is the concentration of the chemical species; t [s] is time; j_{adv} and j_{diff} [$\text{mol}\,\text{s}^{-1}\,\text{m}^{-2}$] are the advective and diffusive fluxes respectively; and G [$\text{mol}\,\text{s}^{-1}$] is the generation or consumption of the chemical species.

In our model we will assume that $G = 0$ as the groundwater is the sole contaminant source and TCE does not readily degrade in soils. However, this term should remain and an appropriate expression developed if one wants to model:

- Biodegradation of some compound in the soil.
- Radon intrusion (remember radon gas is generated in soils and rocks).
- A soil or subsurface source, e.g. a leaky tank or evaporation from a (pure) contaminant spill.

The advective flux is given by

$$j_{\text{adv}} = \vec{u}c \tag{1.21}$$

where $\vec{u}$ [$\text{m}\,\text{s}^{-1}$] is a velocity vector. The diffusive flux is given by Fick's Law

$$j_{\text{diff}} = -D\nabla c \tag{1.22}$$

where D $[\mathrm{m^2\,s^{-1}}]$ is the diffusion coefficient of the contaminant in the solute; and ∇c $[\mathrm{mol\,m^{-3}\,m^{-1}}]$ is a concentration gradient. Thus we get the advection-diffusion equation which generally governs transport of a chemical species

$$\frac{\partial c}{\partial t} + \nabla \cdot (\vec{u}c + -D\nabla c) = 0 \tag{1.23}$$

However, this will not accurately represent contaminant transport in the vadose zone due to

- Contaminant transport occurs inside a variably saturated porous matrix, significantly affecting transport properties.
- The contaminant concentration in the vadose zone will be distributed between three phases - gas, water, and solid (via sorption).

The total contaminant concentration in the soil will be used in lieu of just concentration, i.e. $c \to c_T$ and thus the total contaminant concentration is the sum of the gas, water, and solid phase concentrations.

$$c_T = \theta_w c_w + \theta_g c_g + c_s \rho_b \tag{1.24}$$

Here θ_g and θ_w are the gas-filled and water-filled porosities respectively; c_w and c_g $[\mathrm{mol\,m^{-3}}]$ are the contaminant concentrations in water and gas respectively; c_s $[\mathrm{mol\,kg^{-1}}]$ is the solid phase or sorbed concentration per mass of soil; and $\rho_b = (1-\theta_t)\rho$ $[\mathrm{kg\,m^{-3}}]$ is the bulk density of the soil, which can be calculated from the soil porosity θ_t and solid phase density of the soil ρ $[\mathrm{kg\,m^{-3}}]$.

The attentive reader will now notice that our governing equation depend on three variables instead of one. However, remember that we're concerned with low contaminant concentrations, we can relate the gas and liquid phase concentrations via Henry's Law (1.25)

$$c_g = K_H c_w \tag{1.25}$$

where $K_H = 0.402$ is the dimensionless Henry's Law constant for TCE at 20 °C. We also assume that there are no temperature gradients throughout the vadose zone.

The solid phase concentration can be related to the others via a linear sorption isotherm. Here either the gas-solid or water-solid sorption interaction can be chosen; the former is used in Chapter (TBD) to we will explore effect of gas-solid sorption.

$$c_s = \begin{cases} K_p c_w & \text{Water-solid sorption} \\ K_p c_g = K_p K_H c_w & \text{Gas-solid sorption} \end{cases} \tag{1.26}$$

here K_p $[\mathrm{m^3\,kg^{-1}}]$ is a sorption partitioning coefficient.

Another approach is to simply ignore the role of sorption completely, i.e. $K_p = 0$, which has historically been done in VI modeling and is done in this example too. The reason for this is two-fold.

1. Relevant sorption data has not been available.
2. With an infinite source assumption, and at steady-state, sorption doesn't affect the solution; these have been common assumptions in most VI models so far.

Regardless, we will continue with the sorption K_p term, because this will become relevant in Chapter (TBD) where experimentally derived relevant sorption data is available.

With Henry's Law and the linear sorption assumption we can relate the total contaminant concentration in the soil matrix to the water-phase contaminant concentration.

$$c_T = (\theta_w + \theta_g K_H + K_H K_p \rho_b) c_w \tag{1.27}$$

The terms in front of c_w are collected as $R = (\theta_w + \theta_g K_H + K_H K_p \rho_b)$. This term is called the *retardation factor* and reflects the increased contaminant residence time in the matrix due to shifting between the phases, and becomes an important factor in transient transport simulations.

In the vadose zone, advective transport can occur in both the water and gas phases inside the soil pores.

$$j_{\text{adv}} = \vec{u}_{w,pore} c_w \theta_w + \vec{u}_{g,pore} c_g \theta_g \tag{1.28}$$

here $\vec{u}_{w,pore}$ and $\vec{u}_{g,pore}$ $[\mathrm{m\,s^{-1}}]$ are the water and gas phase *pore* velocities vectors respectively. However, from mass conservation, we know that the product of the pore velocity and porosity gives the superficial velocity of a fluid in porous media, i.e. the Darcy's Law velocities. This together with Henry's Law gives

$$j_{\text{adv}} = (\vec{u}_w + \vec{u}_g K_H) c_w \tag{1.29}$$

and here $\vec{u}_w + \vec{u}_g$ $[\mathrm{m\,s^{-1}}]$ are the Darcy or superficial velocity vectors.

In section 1.3.2 we assumed that there is no gravitational water potential in the soil matrix, and it follows that the water in the pores is stationary, i.e. $\vec{u}_w = 0$ giving

$$j_{\text{adv}} = \vec{u}_g K_H c_w \tag{1.30}$$

where $\vec{u}_g$ is the solution from solving Darcy's Law in section 1.3.3.

To model a scenario where there is a gravitational water potential, one would have to solve two-phase Darcy's Law to get both $\vec{u}_g$ and $\vec{u}_w$. This significantly complicates the mass transport aspect as well, and as such is beyond the scope of this work.

The diffusive transport expression likewise needs to be adjusted, and the total diffusive flux through the pore matrix is given by

$$j_{\text{diff}} = -(D_w \theta_w \tau_w \nabla c_w + D_g \theta_g \tau_g \nabla c_g) \tag{1.31}$$

here $D_w = 1.02 \times 10^{-9}\,\mathrm{m^2\,s^{-1}}$ and $D_g = 6.87 \times 10^{-6}\,\mathrm{m^2\,s^{-1}}$ are the contaminant diffusion coefficients of TCE in pure water and gas respectively; and τ_w and τ_g are the water and gas tortuosity terms.

Due to the irregular shapes of pores, diffusion of a chemical species will inevitably often occur along a tortuous path, which the tortuosity terms attempt to capture. As tortuosity depend on the structure of the porous matrix, it is difficult to accurately portray, but a popular approach is to use Millington & Quirks model[5].

$$\tau_w = \frac{\theta_w^{\frac{7}{3}}}{\theta_t^2},\ \tau_g = \frac{\theta_g^{\frac{7}{3}}}{\theta_t^2} \tag{1.32}$$

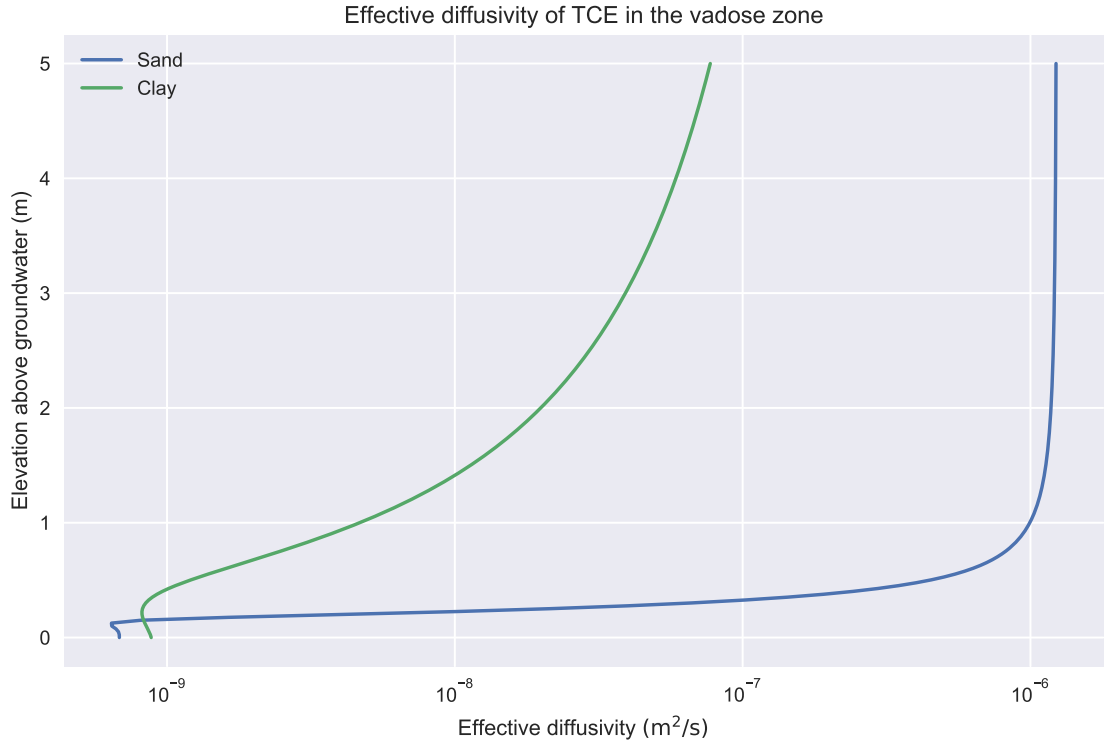

Figure 1.6: Effective diffusivity of TCE in the vadose zone using Millington-Quirks model. Soil water and gas filled porosites are calculated using van Genuchten's equations.

here θ_t is the total or saturated porosity of the soil matrix. Another popular approach is Bruggeman's model, or if possible, a custom version can be used.

Combining (1.32) and (1.25) in our diffusion flux expression gives

$$j_{\text{diff}} = -\left(D_w \frac{\theta_w^{\frac{10}{3}}}{\theta_t^2} + D_g \frac{\theta_g^{\frac{10}{3}}}{\theta_t^2} K_H\right) \nabla c_w \tag{1.33}$$

the terms in front of ∇c_w can be collected as an effective diffusion coefficient D_{eff} $[\text{m}^2\,\text{s}^{-1}]$, which with our isothermal vadose zone assumption only depends on the soil moisture content. Thus we get the final diffusive flux expression

$$j_{\text{diff}} = -D_{\text{eff}} \nabla c_w \tag{1.34}$$

Figure 1.6 shows how the effective diffusivity varies from being close to that of the pure water diffusivity near the capillary zone, and increases to something closer to gas-phase diffusivity as the soil moisture decreases.

Putting all this together finally gives us the governing equation for contaminant transport in the vadose zone for our modeled VI scenario.

$$R\frac{\partial c_w}{\partial t} = \nabla \cdot (D_{\text{eff}} \nabla c_w) - K_H \vec{u}_g \cdot \nabla c_w \tag{1.35}$$

To solve this we need to define some boundary and initial conditions.

Boundary Conditions In this VI scenario, the sole contaminant source is assumed to be the homogenously contaminated groundwater, which we assume to have a fixed concentration. The atmosphere acts as a contaminant sink and thus this is simply a zero concentration boundary condition. Contaminants leave the soil domain and enter the building through a combination of advective and diffusive gas phase transport. The boundary condition applied to all other boundaries is a no-flow boundary.

Atmosphere	$c_w = 0\,\mathrm{mol\,m^{-3}}$	(1.36)
Groundwater	$c_w = c_{gw} = 0.1\,\mathrm{mol\,m^{-3}}$	(1.37)
Foundation crack	$-\vec{n}\cdot\vec{N} = \dfrac{-j_{ck}}{K_H}\ \mathrm{mol\,m^{-2}\,s^{-1}}$	(1.38)
All other	$-\vec{n}\cdot\vec{N} = 0\,\mathrm{mol\,m^{-2}\,s^{-1}}$	(1.39)

$\vec{n}\cdot\vec{N}$ is the dot product between the boundary normal vector and the contaminant flux; j_ck is the contaminant vapor flux into the building. We assume that only contaminants in the gas phase enter the building, and dividing j_{ck} by K_H we get proper accounting in terms of the water phase concentration accounting in the main transport equation 1.35.

Initial Conditions For steady-state problems, the initial conditions do not influence the solution. Transient simulations however, require initial conditions and these are assumed to be given by the steady-state solution.

Basis function A second order polynomial (quadratic) function is used as the basis function for solving the transport equation.

1.4 Meshing

The mesh in FEM model is the collection of small discrete elements make up the model geometry or domain. Meshing is the process of generating a mesh. Meshing is one of the most important aspects of FEM modeling as the mesh directly influences the accuracy of the solution; it is important that the various gradients are resolved by the mesh. However, designing a good mesh can be challenging as a finer mesh has a higher computational cost. A good mesh designer must constantly balance accuracy and computational costs by considering where a mesh can be finer and where it can be coarser.

The most fundamental unit of the mesh is the element(s) that comprise the mesh. There are many different types of elements that can be used for meshing and choosing which ones to use depend primarily on the spatial dimensionality of the model, the particularities of the geometry, and the physics that we wish to model. Obviously different element types are by necessity needed to model a 2D vs. 3D geometry; you cannot mesh a 3D geometry with 2D squares.

There are primarily four types of 3D mesh elements available - the tetrahedral, cuboid, prism, and pyramid. These can be combined in various ways to represent any 3D geometry. The most general 3D element is the tetrahedral and will approximate any geometry well. However, it is not always the most effective choice for meshing a

geometry and another element type may be better suited. This is easiest illustrated with an example.

Imagine that you are trying to simulate the laminar flow of some fluid in a pipe. Because of symmetry, only a wedge of the pipe needs to be explicitly modeled. Therefore, in this scenario, it might be beneficial to use prism elements rather than tetrahedrals, since these are already wedge shaped.

The laminar pipe flow is also going to primarily have a gradient in the direction of the flow. Thus the mesh mostly only needs to be fine in the flow direction, while the mesh can be coarser in the orthogonal direction. Constructing a mesh on this basis would allow us to achieve a solution of high accuracy while still keeping the number of elements relatively small - all through clever mesh design.

This is of course a relatively simple example and more complicated geometries may need all kinds of element for constructing a clever design. These type of multi-element meshes can give significant computational saving but at the expense of often requiring significant user input to be generated. Sticking to one type of elements is often simpler as these can quickly and easily mesh geometries.

Meshing can be done manually, but is often performed by a meshing algorithm. The creation of these algorithms is a science in itself, but their use often involve passing some basic parameters to the algorithm. Here the user could, for instance, specify the maximum and minimum element sizes, max element growth rate, how finely small features or curves (typically quite difficult to mesh) should be meshed. These instructions can be specific to various parts of the model, e.g. much finer meshing resolution can be specified for an area of interest and vice versa. There are also a variety of specialty mesh features such as a mesh boundary layer available: adding finely spaced mesh layers along a boundary. How to use all of these tools effectively to mesh a geometry is why meshing can be one of the most challenging aspects of FEM modeling.

1.4.1 Meshing The VI Model

Now that we know a little about meshing in general, we can move on and mesh our VI model geometry. The first choice we need to make is which type of element to use, and in order to do that we need to think about the gradients of the dependent variables.

From van Genuchten's retention curves, we know there will be a large soil moisture gradient in the capillary zone, which will need a relatively fine mesh to be resolved. The airflow from Darcy's Law will forming some sort of arcing streamline from the ground surface to the foundation crack; the pressure gradient will be inline with these streamline. The concentration gradient is difficult to predict a priori, but there likely will be some gradient from the groundwater to the ground surface and foundation crack. Since many of these gradients intersect and go in different directions from each other it makes sense to use tetrahedral elements to mesh the geometry; these are the more general 3D elements.

Properly meshing our geometry can be a challenge due to the great range of geometric scale. The house and soil domains are on the order of meters while the foundation crack is only 1 cm side, and requires very fine meshing. This is not only due to its small size, but because the contaminant entry will be calculated based on the solution here, which largely determines the indoor contaminant concentration.

The COMSOL meshing algorithm only require a few parameters to relatively mesh a geometry with tetrahedrals. A description of each parameter and its value can be seen in Table 1.1.

Table 1.1: Inputs to COMSOLs meshing algorithm.

Input	Value	Description
Maximum element size	1.5 m	Maximum size of a element
Minimum element size	1 mm	Minimum size of a element
Maximum element growth rate	1.3	Maximum allowed size increase of adjacent elements. 1.3 indicates that an element can only be 30% larger than its neighbor. A smaller value gives a finer mesh.
Curvature factor	0.4	Ratio between the boundary element size and the geometry curvature radius. A smaller value gives a finer mesh.
Resolution of narrow regions	1	Control the number of layers of elements that are created in narrow regions. A larger value gives a finer mesh.

1.4.2 Boundary Layer Mesh

When posed with steep gradients in one particular direction at boundaries, as we are here, it is often useful to use a *boundary layer mesh* at the impacted boundaries. This is a type of mesh that introduces a dense layer of meshes along the normal direction from a boundary. The number of layers are supplied by the user, and in our case we will use 8 layers, but more could be added if needed. The distance between each layer is determined by the size of the other elements in its vicinity, as well as the distance growth rate between each layer, which we set to 1.3, i.e. the distance increases by 30% for each layer. Figure 1.7 shows our completed mesh.

1.5 Solver Configuration

A solver(s) is required to solve the VI model, and a few considerations need to be taken when choosing one. For simplicity we will now first consider a stationary or steady-state problem. Since our model is a multiphysics problem, i.e. many of the physics depend on each other, we first need consider how to couple our physics. The physics can be coupled by either using a *segregated* or *fully coupled* approach.

Segregated vs. fully coupled physics In a segregated solver, each governing equation or physics is solved separately in a specific order. For instance, in our VI example we could solve Darcy's Law first, get some solution, then use that in the transport equation, solve that, and then solve the indoor concentration equation, i.e. we solve one system of equation per physics. These steps are simply iterated until convergence occurs in all of the separated steps. The fully coupled approach assembles a single large system of equation from all of the physics. Both of these

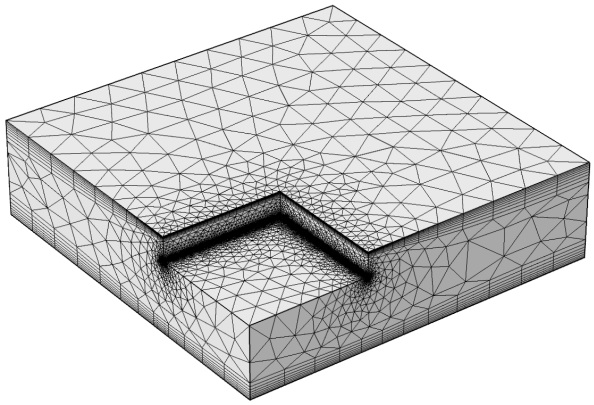

(a) The darker perimeter around the foundation highlights the higher mesh density along the foundation crack.

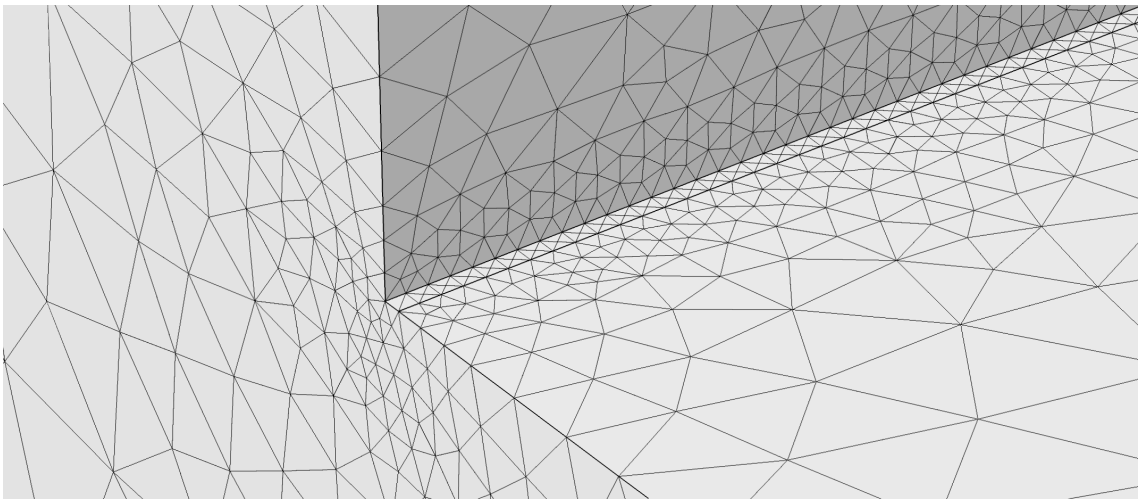

(b) Close-up of the foundation crack mesh.

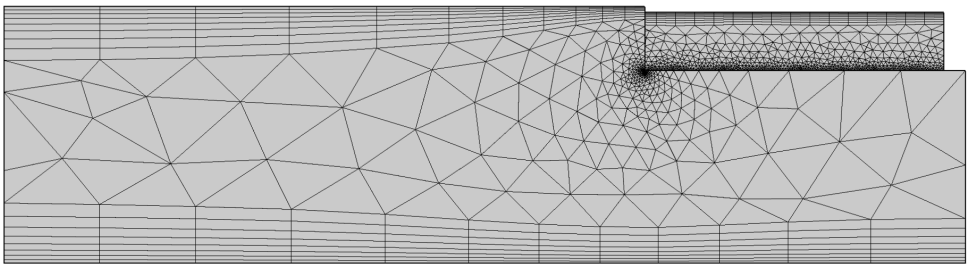

(c) Side-view highlighting the boundary layer mesh.

Figure 1.7: Initial mesh of our geometry.

approaches will reach the same solution, but the fully coupled approach will do so faster, but at the expense of using more memory.

Direct vs. iterative solver Within each of these coupling approaches, we need to specify a solver to solve the system of equations. Here we are again faced with a choice, and we could either use a *direct* or *iterative* solver. Direct solvers, as the name implies, arrive at a solution directly and are based on LU-decomposition. Iterative solvers on the other hand, iteratively approach the solution, and are based on conjugate gradient method. The advantage of direct solvers is that they are faster, but use more memory, while iterative solvers are slower but use less memory. In terms of choosing a solver algorithm, there are many options, but MUMPS and GMRES will be used as the respective algorithm for direct and iterative solvers.

Time-dependent solvers To solve a transient or time-dependent problem (which will be done in subsequent chapters) a solver to step forward in time is required. A too large time step will cause stability issues and ultimately convergence will be impossible, but obviously some discrete time step is required for a solution to be achievable. A time-dependent solver picks an appropriate time-step and there are some popular approaches, such as using some high-order Runge-Kutta (RK) or backwards differentiation formula (BDF). Regardless of the type of solver, for each time step the system of equations will be solved using one of the aforementioned solvers. The difference between RK and BDF is that RK explicitly discretizes time while BDF does so implicitly. In this work we will only use BDF as it is more stable than RK.

Choosing solvers The choice of solver will not affect (or should not at least) the solution to the problem. However, it can have a large impact on computational time and resources, and these considerations dictate solver choice (this is also partially dependent on the mesh used, as this will affect memory usage too). In this example, and throughout the models used in this work, we will favor speed over memory and therefore fully couple all our equations and use direct solvers.

1.5.1 Adaptive Mesh Refinement

The accuracy of the solution obtained by FEM is dependent on the quality of the mesh, something that was discussed in section 1.4. While the mesh designer can do much to create a mesh that performs well for the particular problem posed, refinement of the mesh is often needed and should be performed for every new model.

There are two types of mesh refinements in FEM. The first type reduces the size of the elements and thereby the accuracy of the solution, this is called *h-type* refinement (h is often used to denote the mesh size). The second increases the order of the polynomial of the basis function, called *p-type* refinement which will likewise increases the solution accuracy.

h-type refinement is generally more attractive because it is simpler and the computational cost of p-type refinement increase faster than h-type. However, p-types are useful if the user imports an already existing mesh, and is unable to change it, rendering h-type refinement impossible. These two method can be combined to perform a *hp-type* refinement.

Refinement is usually done by an algorithm, which is possible because FEM has the built-in ability to estimate the local error of the solution anywhere in the

domain. The downside with using an algorithm is that the user has little control over how the mesh is refined. The user can also manually refine the mesh by solving the model and plot how some relevant metric converges as the mesh is refined. This can be a very time consuming, and therefore algorithms are usually preferable; a hybrid solution is to manually alter the mesh after the algorithmic mesh refinement.

Refinement can either be done locally or globally. Global refinement involves defining some singular metric that will be used to evaluate the quality of the mesh, e.g. one might use the total stress in a metal bar as a metric here. In local refinement, one still has to define some metric for evaluating the quality of the refinement, but evaluation only occurs on a subset of the domain, e.g. the stress on just one boundary of the same metal bar. In both approaches the elements that have the largest estimated local error are refined; this error estimation is an inherent feature of FEM. The optimal type of refinement varies by problem, but a global refinement will generally be more computationally expensive.

In this work we will use a global h-type refinement and use the indoor contaminant concentration c_{in} as our refinement metric. COMSOLs refinement algorithm has the nice ability to reinitialize the mesh, and can thereby coarsen elements, i.e. increase h where the local error is very small. This is handy as a fine mesh is not needed far away from the foundation crack - saving computational resources. In this example we will tell the algorithm to refine the mesh three times, and stop if the total number of elements exceed 1 million, with a maximum coarsening factor of 3, and element growth rate of 1.7, i.e. the number of elements increase by roughly 70% each iteration.

The result of this refinement can be seen in Figure 1.8 where the original and refined mesh are juxtaposed. Notice how the mesh is now denser near the foundation, the boundary layers tighter (in particular near the groundwater boundary), and how the elements are larger in the periphery. The original and refined meshes has 362,657 and 1,065,743 elements respectively.

1.6 Post-processing & Results

One of the benefits of using a FEM software like COMSOL is its advanced post-processing capabilities. This allows the user to examine the physics driving VI in great detail. Figure 1.9 shows the resulting pressure field from solving Darcy's Law, as well as the associated airflow streamlines in the soil. Here we see the pressure in the near foundation crack region is roughly the same as the house pressurization of $-5\,\mathrm{Pa}$, which quickly decreases towards the ground surface. It is also apparent how this pressure field induces a airflow from the ground surface, with air near the house heading relatively straight to the foundation crack, whereas the air further away from the house penetrates deeper into the soil and almost "whirlwinds" underneath the house.

The contaminant concentration in the soil, normalized to the groundwater source concentration and log-transformed, with the contaminant flux streamlines, is examined in Figure 1.10. Here see that far away from the house, the contaminant vapor simply diffuse straight from the groundwater source to the atmosphere, while these accumulate underneath the house, which acts as a diffusion blocker. Bases on those streamlines we can conclude that the advective component of the flux is very here small. Perhaps surprisingly, we do not see a significant advective transport down-

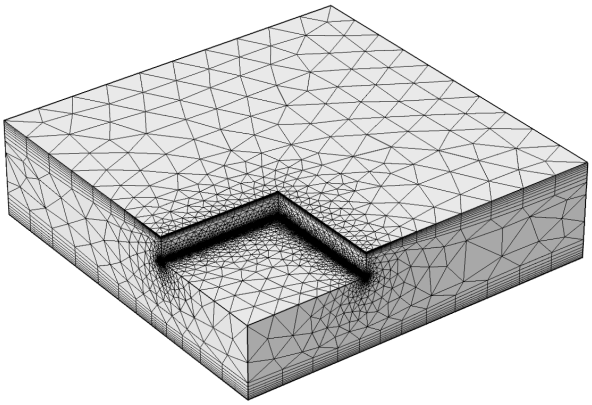

(a) Original mesh. 362,657 elements.

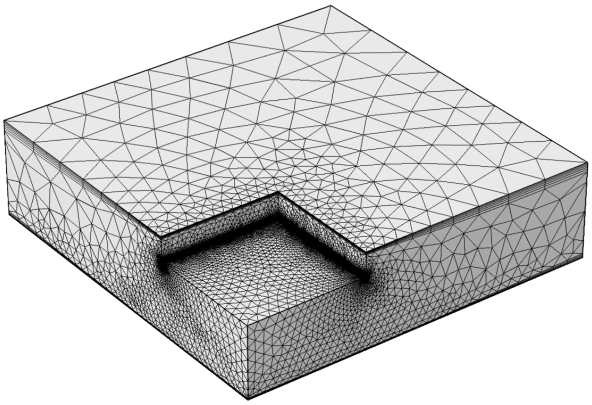

(b) Refined mesh after two steps of global refinement w.r.t. the indoor contaminant concentration. 1,065,743 elements.

Figure 1.8: Original and refined mesh.

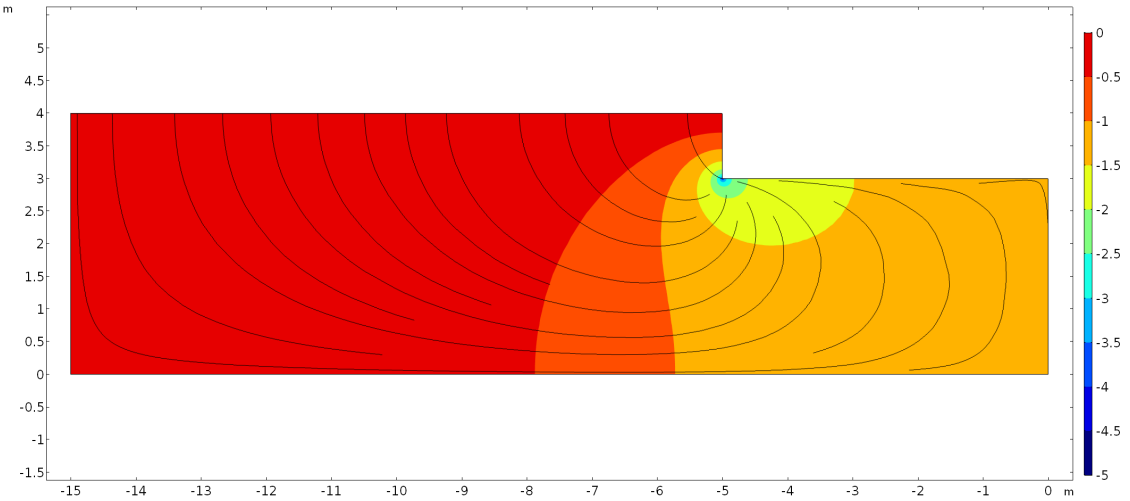

Figure 1.9: Pressure field from Darcy's Law with associated airflow streamlines.

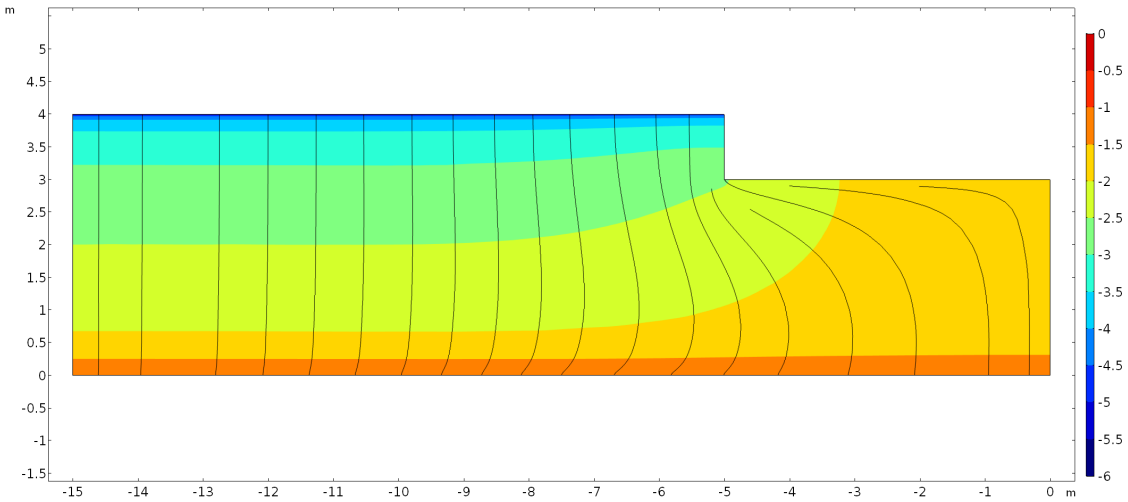

Figure 1.10: Contaminant concentration in the soil, normalized to groundwater concentration and log-transformed, with transport streamlines.

wards along the wall of the house. However, considering the soil type is sandy loam, airflow velocities are expected to be small.

One might think that advective transport is large in the horizontal direction along the foundation slab, as the transport and airflow streamlines are so similar. However, by inspecting Figure 1.11 we see that airflow velocities are not great here than elsewhere, and therefore the advective transport is not either. To make sense of this, we can inspect the horizontal diffusive flux, divided by the magnitude of the total flux

$$\frac{j_{\text{diff,y-direction}}}{|j_{\text{total}}|} \tag{1.40}$$

to see what portion of the total transport the diffusive horizontal make up here. The results of this is shown in Figure 1.12, where see that the horizontal diffusive flux in the left direction accounts for 80% of the total flux magnitude, as indicated by -0.8. This shows the power of modeling and how it can reveal things that at first seem intuitively correct, but in fact are not.

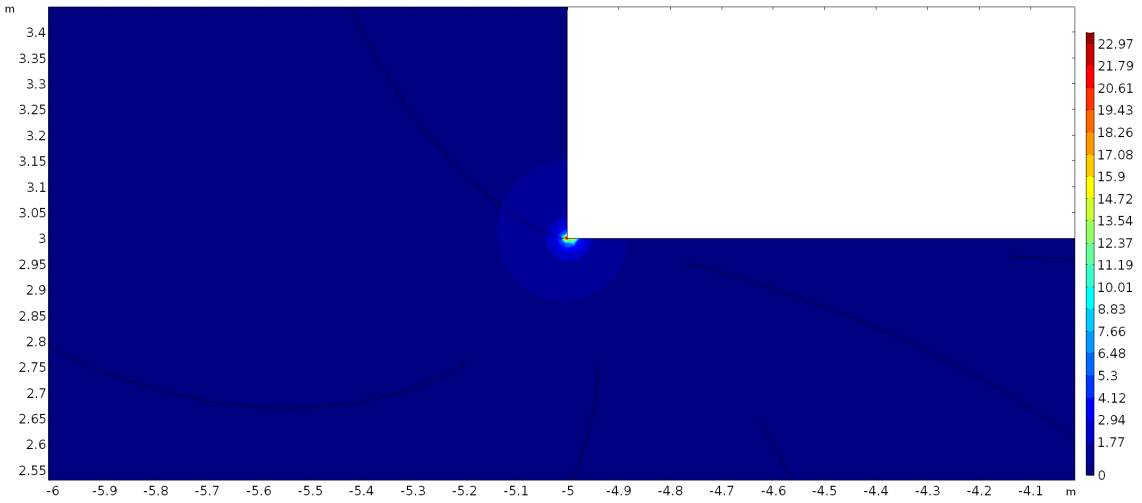

Figure 1.11: Airflow velocity [mm h^{-1}] near the foundation crack with associated its streamlines.

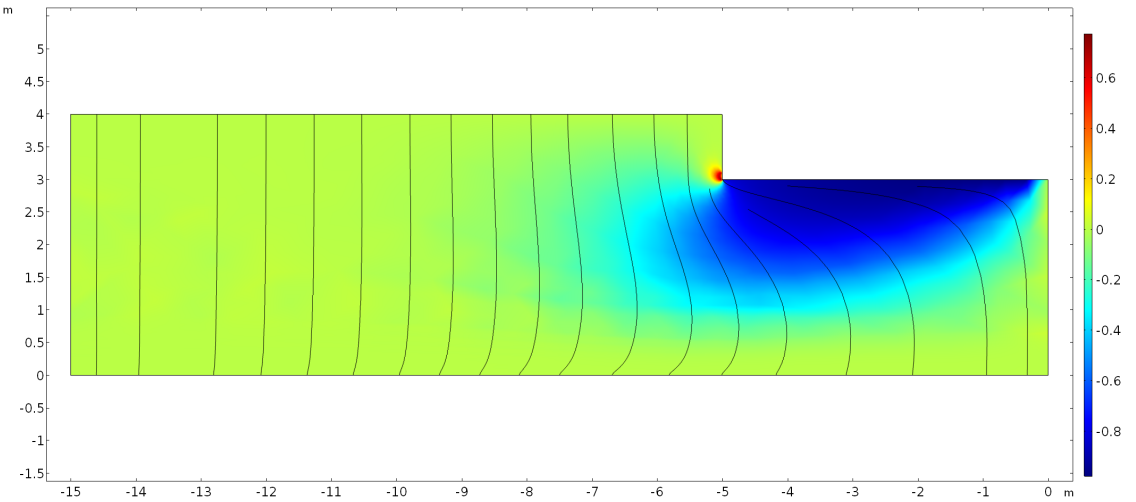

Figure 1.12: Horizontal diffusive flux component of the magnitude of the total flux. 1 here would indicates that all of the contaminant transport is due to diffusion, and occurs solely in the rightwards direction.

Another useful feature of post-processing is that it can be used for bug searching and to evaluate where the mesh can be potentially improved. The when numerically the transport equation used to model contaminant transport, there is a tendency for the solution to oscillate around the "true" solution, and thereby violate mass conservation, if the mesh size in a particular element is too large. This can be quantified by the cell Péclet number, which characterizes the relative magnitude of advection/diffusion in a cell.

$$\mathrm{Pe}_{\mathrm{cell}} = \frac{\mathrm{adv}_{\mathrm{cell}}}{\mathrm{diff}_{\mathrm{cell}}} = \frac{u_g h}{2D_{\mathrm{eff}}} \tag{1.41}$$

here u_g [$\mathrm{m\,s^{-1}}$] is the soil-gas airflow velocity; h [m] is the mesh size in the element or cell; and D_{eff} [$\mathrm{m^2\,s^{-1}}$] is the effective diffusivity in the cell. If $\mathrm{Pe}_{\mathrm{cell}} > 1$ there is a risk that this oscillating behavior will manifest. Small exceedances, $\mathrm{Pe}_{\mathrm{cell}} < 25$, are usually able to be mitigated by various stabilization schemes, which are inherently integrated into COMSOL as well as many other FEM packages, but for larger values further mesh refinement may be required.

Figure 1.13 shows $\mathrm{Pe}_{\mathrm{cell}}$ as a volume plot, and excludes all values that fall below one. As we can see, only the region close to the groundwater exceeds $\mathrm{Pe}_{\mathrm{cell}}$, which is due to the very small D_{eff} there. The exceedance is small, so the stabilization scheme is able to compensate which is confirmed by Figure 1.10 (no oscillations visible). This is also a region where even if such oscillations occurred, would probably not affect the indoor contaminant concentration. Regardless, Figure 1.13 shows where the mesh may potentially be refined, which comes in handy to know if one runs a model where airflow velocities are significantly higher than in this example.

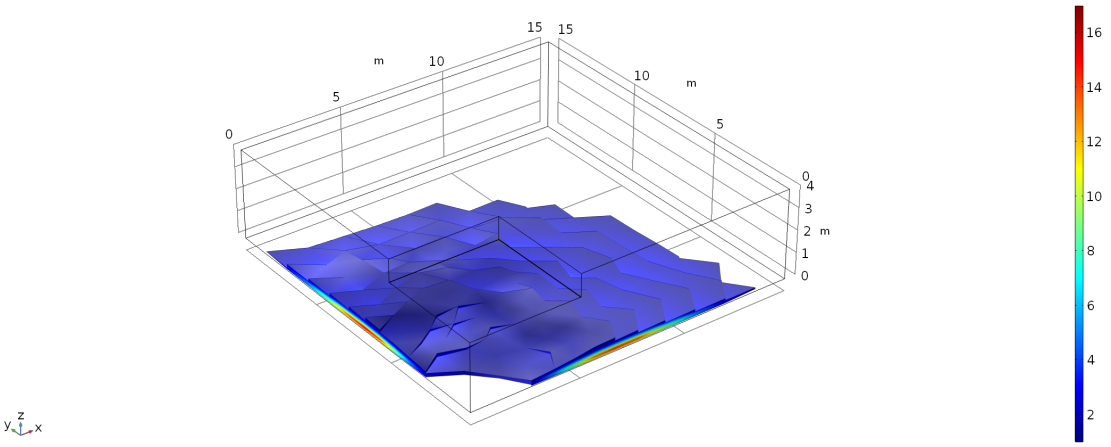

Figure 1.13: Volume plot showing where the cell Péclet number exceeds 1 and its actual value. I.e. it suggests where the mesh may be improved.

Table 2: Properties and van Genuchten parameters of select soil types[6].

Soil type	Permeability κ (m^2)	Density ρ (kg/m^3)	Porosity θ_t	Residual moisture θ_r	van Genuchten parameter α	van Genuchten parameter m
Sand	9.9×10^{-12}	1430	0.38	5.3×10^{-2}	3.5	3.2
Loamy sand	1.6×10^{-12}	1430	0.39	4.9×10^{-2}	3.5	1.7
Sandy loam	5.9×10^{-13}	1460	0.39	3.9×10^{-2}	2.7	1.4
Sandy clay loam	2.0×10^{-13}	1430	0.38	6.3×10^{-2}	2.1	1.3
Loam	1.9×10^{-13}	1380	0.40	6.1×10^{-2}	1.5	1.5
Silt loam	2.8×10^{-13}	1380	0.44	6.5×10^{-2}	0.51	1.7
Clay loam	1.3×10^{-13}	1500	0.44	7.9×10^{-2}	1.6	1.4
Silty clay loam	1.7×10^{-13}	1390	0.48	9.0×10^{-2}	0.84	1.5
Silty clay	1.5×10^{-13}	1300	0.48	1.1×10^{-1}	1.6	1.3
Silt	6.7×10^{-13}	1260	0.49	5.0×10^{-2}	0.66	1.7
Sandy clay	1.7×10^{-13}	1470	0.39	1.2×10^{-1}	3.3	1.2
Clay	2.3×10^{-13}	1330	0.46	9.8×10^{-2}	1.3	1.3
Gravel[7]	1.3×10^{-9}	1430	0.42	5.0×10^{-3}	100	2.19

Bibliography

[1] Mats G. Larson and Fredrik Bengzon. *The Finite Element Method: Theory, Implementation and Applications*. Springer, 2010.

[2] Chase Holton et al. "Creation of a Sub-Slab Soil Gas Cloud by an Indoor Air Source and Its Dissipation Following Source Removal". en. In: *Environ. Sci. Technol.* 52.18 (Aug. 2018), pp. 10637–10646. ISSN: 0013-936X, 1520-5851. DOI: 10/gd569z.

[3] R. H. Brooks and A. T. Corey. "Properties of Porous Media Affecting Fluid Flow". In: *J. Irrig. Drainage Div.* 72.2 (1966), p. 61.

[4] M. Th. van Genuchten. "A Closed-Form Equation for Predicting the Hydraulic Conductivity of Unsaturated Soils". In: *Soil Sci. Soc. Am.* 44.5 (1980), pp. 892–898. DOI: 10/fdc8mc.

[5] R. J. Millington and J. P. Quirk. "Permeability of Porous Solids". In: *Trans. Faraday Soc.* 57.0 (Jan. 1961), p. 1200. DOI: 10/btx653.

[6] Lilian D V Abreu and Henry Schuver. *Conceptual Model Scenarios for the Vapor Intrusion Pathway*. en. 2012.

[7] Han-Cheng Dan et al. "Capillary Effect on Flow in the Drainage Layer of Highway Pavement". In: *Can. J. Civ. Eng.* 39.6 (June 2012), pp. 654–666. ISSN: 0315-1468. DOI: 10/f3236b.